

24 coefficient in summer is only 0.33. As expected, the monthly mean RT and LRT height
25 both show seasonal variations. Lomb-Scargle periodograms show that the tropopause
26 exhibits obvious diurnal variation throughout the seasons, whereas the semidiurnal
27 oscillations are rare and occasionally observed during summer and later spring. Our
28 study shows the good capability of the Beijing MST radar to determine the tropopause
29 height, as well as present its diurnal oscillations.

30 **Key words:** VHF radar; MST radar; tropopause; diurnal oscillation.

31

32 **1. Introduction**

33 The tropopause marks a transition zone separating the well-mixed convectively
34 active troposphere from the stably stratified and more quiescent stratosphere. Its
35 structure and variability is characterized by large changes in thermal (e.g., lapse rate),
36 dynamical (e.g., potential vorticity), and chemical properties (e.g., ozone and water
37 vapor) and hence acts as a key role for the stratosphere-troposphere exchange (STE)
38 processes (Hoinka, 1998; Seidel et al., 2001). The height of the tropopause depends
39 significantly on the latitude, with about 17 km near the equator and less than 9-10 km
40 at polar latitudes (Ramakrishnan, 1933). Over subtropical latitudes with the presence
41 of subtropical jet, where the tropopause experiences rapid change or breaking,
42 tropopause folding events are commonly observed (Pan et al., 2004). Climatologically,
43 the altitude of the tropopause represents the seasonal variation of the flux of
44 stratospheric air intruding into the troposphere (Appenzeller et al., 1996). Moreover,
45 the tropopause height trends can be a sensitive indicator of anthropogenic climate

46 change (Sausen and Santer, 2003; Santer et al., 2003a; Añel et al., 2006).

47 A variety of ways are available to determine the extratropical tropopause.
48 Radiosonde sounding is the most commonly used to define the thermal tropopause
49 (hereafter referred to as LRT) based on temperature lapse-rate (WMO, 1957). The
50 thermal definition of tropopause can be applied globally and the tropopause height
51 easily be determined from one individual profile (Santer et al., 2003). ~~Radiosonde
52 sounding, however, is impracticable in severe weather conditions such as intense
53 rainfall and cold air outbreak.~~ Another feasible definition is to use a specific potential
54 vorticity (PV) surface to represent the dynamical tropopause (hereafter referred to as
55 PVT) (Reed, 1955; Hoskins et al., 1985). Dynamical definition has the advantage that
56 the PV is a conserved property (under adiabatic and friction-less conditions) of an air
57 mass (Hoskins et al., 1985; Bethan et al., 1996). Values in the range 1-4 PVU (1 PVU=
58 $10^6 \text{ m}^2 \text{ s}^{-1} \text{ K kg}^{-1}$) are used in previous researches in the Northern Hemisphere
59 (e.g. Baray et al., 2000; Sprenger et al., 2003; Hoerling et al., 1991). The threshold of
60 2 PVU surface is the most commonly used (Gettelman et al., 2011). Dynamical
61 definition, however, is not applicable near the equator, where the PV tends to be 0 (e.g.,
62 Hoerling et al., 1991; Nielsen-Gammon et al., 2001). Creating a blended tropopause
63 globally may probably a good way forward (Wilcox et al., 2011). In addition, the data
64 of GPS radio occultation satellites is also an effective way and commonly applied to
65 study tropopause (e.g. Schmidt et al., 2005; Son et al., 2011).

66
67 As a result of partial specular reflection from stable atmospheric layer, the radar

68 tropopause (RT) can be well represented and identified by atmospheric radars operating
69 at meter wavelength (VHF band) and directing at vertical incidence (Gage and Green,
70 1979). Research activity increased remarkably following the first report on VHF radar
71 detection of tropopause by Gage and Green (1979), for instance, the researches in
72 middle latitudes (e.g. Hermawan et al., 1998), polar regions (e.g. Hall, 2013a), and
73 tropical regions (e.g. Das et al., 2008; Ravindrababu et al., 2014). Several methods have
74 been proposed to determine the tropopause height via radar echo power, including the
75 largest gradient in echo power (Vaughan et al., 1995; ~~Alexander et al., 2012~~ [Alexander
76 et al., 2013](#)), the maximum echo power (Vaughan et al., 1995; Hall et al., 2009), and
77 the specific value of echo power (Gage and Green, 1982; Yamamoto et al., 2003). The
78 method of the RT height determination used in this paper will be described in detail in
79 next section.

80 The biggest advantage of the VHF radar measurements is the ability of continuous
81 operation unmanned in any weather conditions. Of course, no definition of the
82 tropopause is perfect. VHF radar system can only be limited to a few locations globally.
83 A detailed review of the close relationship between these different tropopause
84 definitions is provided by Alexander et al., (2012).

85 By means of the radiosonde, reanalysis, and satellite data available globally, long-
86 term (annual or longer) variability in tropopause height has received extensive attention
87 (e.g. Randel et al., 2000; Angell and Korshover, 2009; Son et al., 2011; Liu et al., 2014).
88 However, short period (diurnal or semidiurnal) variability of the tropopause is hard to
89 be examined by these measurements. In contrast, benefiting from the much higher

90 temporal resolution, radar definition of the tropopause provides good capability for
91 studying the diurnal and semidiurnal variation in tropopause height. Earlier, Yamamoto
92 et al., (2003) reported the capability of the Equatorial Atmospheric Radar to examine
93 the diurnal variation of tropopause height. Then, the diurnal variability of the tropical
94 tropopause was investigated in detail by Das et al., (2008) using the Indian Gadanki
95 MST radar. Its diurnal variation over a polar latitude station was investigated by Hall
96 (2013b). In the absence of pressure and temperature parameters, the evidence of
97 atmospheric tides can be well represented by winds (e.g. Huang et al., 2015).

98 The tropopause structure in midlatitudes is different from that in other regions.
99 Double tropopauses structure is a ubiquitous feature over mid-latitude regions near
100 40°N (Pan et al., 2004; Randel et al., 2007). Strong evidence has revealed that the
101 poleward intrusion of subtropical tropospheric air that occurred above the subtropical
102 jet have resulted in the double structure (Pan et al., 2009). The higher part (second
103 tropopause near ~16 km) is characterized by tropical features of cold and higher level,
104 whereas the lower part (first tropopause near ~12 km) is characterized by polar features
105 of warm and lower level. In the present study, we focus only on the first tropopause
106 (below 16 km, if it exists) which will be referred to as ‘tropopause’ hereafter.

107 ~~So far, knowledge on the high temporal resolution (within 1 hour) structure and~~
108 ~~variability of the midlatitude tropopause is still insufficient.~~ In this study, using more
109 than 5 years of Beijing MST radar echo power measurements in vertical beam, we
110 mainly focus on the high-resolution characteristics of the tropopause structure and their
111 comparison with the simultaneous radiosonde and dynamical definitions. Another

112 important objective of this study is to examine the diurnal and semidiurnal variability
113 of the tropopause. The observational characteristics of e.g. winds, echo power, and data
114 acquisition rate near the tropopause layer are also presented in the paper.

115

116 **2. Data and Methods**

117 **2.1. Radar Dataset**

118 As an important part of the Chinese Meridian Project, two MST radar systems are
119 designed and constructed to improve the understanding of the extratropical troposphere,
120 lower stratosphere, and mesosphere (Wang, 2010), which are Wuhan and Beijing MST
121 radars. The Beijing MST radar located in Xianghe, Hebei Province, China (39.75° N,
122 116.96° E, 22 m above sea level) was designed and constructed by the Institute of
123 Atmospheric Physics, Chinese Academy of Sciences and started its routine operation
124 since 20 October 2011 (Tian and Lu, 2017). The radar is a high power coherent pulse-
125 Doppler radar operating at 50 MHz with the maximum peak power of 172 kW and the
126 half-power beam width of 3.2° . Five beams are applied: one vertically pointed beam
127 and four 15° off-zenith beams tilted to north, east, south, and west. In order to obtain
128 the high-quality measurements from troposphere, lower stratosphere, and mesosphere
129 simultaneously, the radar is designed to operate routinely in three separate modes: low
130 mode (designed range 2.5--12 km), middle mode (10--25 km), and high mode (60--90
131 km) with vertical resolutions of 150, 600, and 1200 m, respectively. Under the routine
132 operation, the 15-min break is followed by the 15-min operation cycle (5 min for each
133 mode). As a result, the time resolutions of the low, middle, and high mode

134 measurements are all 30 min. More detailed review of the radar system is given by
135 Chen et al. (2016).

136 Here only the low mode echo power measurements are used to determine the RT
137 height. Although the designed detectable range of the low mode is from 2.5~12 km,
138 the vertically pointed beam can receive stronger echoes from a higher level (~14-15 km)
139 as compared with those from off-vertical beams due to the partial specular reflection
140 mechanism. The measurements in middle mode are also applied to calculate the winds
141 or echo power within ~5-6 km of the tropopause. The parameters for the two routine
142 operation modes are listed in Table 1. The monthly total number of the echo power
143 profiles available in vertical beam (low mode) is shown in Fig. 1. The outliers or
144 severely contaminated data that mainly induced by system problems are eliminated.
145 The large data gap in September is due to the annual preventive maintenance.

146 **2.2. Tropopause Definitions**

147 Due to the large gradient in potential temperature, radar return power received at
148 vertical incidence is significantly enhanced upon the transition zone of the tropopause
149 layer. Using this characteristic, the RT height can be determined effectively by the VHF
150 radar. Here, the RT is defined as the altitude (above 500 hPa) where the maximum
151 vertical gradient of echo power is located (Vaughan et al., 1995; ~~Alexander et al., 2012~~
152 [Alexander et al., 2013](#); Ravindrababu et al., 2014; Chen et al., 2018). Considering the
153 occasional and random noise, to which the derived-RT is sensitive, the echo power
154 profiles are smoothed by a 3-point running mean. In order to further reduce the
155 influence of the noise, the RT definition used here need to satisfy an additional criterion:

156 the determined RT height should be continuous with the adjacent RT heights (one on
157 each side), otherwise to search for the second peak gradient (eliminated if the second
158 peak does not meet the additional criterion). The “continuous” here means that the
159 discrepancy between the two successive heights (in time, 0.5-hour interval) should be
160 <0.6 km. A typical example of the RT and LRT is illustrated in Fig. 2. The LRT is
161 identified based on the World Meteorological Organization (WMO) criteria (WMO,
162 1957). The radar aspect sensitivity is expressed as the ratio between vertical (p_v) and
163 oblique (p_o) beam echo power (here is 15° east beam). The radiosonde soundings are
164 launched twice daily from the Beijing Meteorological Observatory (39.93 °N, 116.28
165 °E, station number 54511), which is less than 45 km to the radar site. In this case, the
166 LRT and RT consistent well and are at 11.65 km and 11.85 km respectively. As expected,
167 the LRT characterized by a rapid increase in potential temperature gradient also
168 corresponds to the large gradient in radar aspect sensitivity. Note that the height with
169 maximum value in echo power lie at a higher altitude (as compared with the RT height)
170 of ~700 m above the LRT. The dynamical tropopauses used in this paper are derived
171 from the European Centre for Medium-Range Weather Forecasts (ECMWF) ERA-
172 Interim Reanalysis (Dee et al., 2011) and defined as the surface of 2 PVU potential
173 vorticity, which is same to that used by Sprenger et al., (2003) and Alexander et al.
174 (~~2012~~2013).

175 **2.3. Tropopause sharpness definition**

176 For the compared data pairs between the RT and LRT, we calculate the
177 corresponding tropopause sharpness that represents the strength of the tropopause

178 inversion layer. As defined by Wirth, (2000), the tropopause sharpness S_{TP} can be
179 calculated as:

$$180 \quad S_{TP} = \frac{T_{TP+\Delta z} - T_{TP}}{\Delta z} - \frac{T_{TP} - T_{TP-\Delta z}}{\Delta z} \quad (1)$$

181 where TP denotes the tropopause height, $\Delta z = 1$ km, and T_{TP} indicates the
182 corresponding temperature. This definition is also used in Alexander et al. [2012-2013](#)
183 and we're using it for a good comparison with our results.

184

185 **3. Results**

186 **3.1. High-resolution radar tropopause structure**

187 The fine-scale height-time cross section of radar echo power and aspect sensitivity
188 is shown in Fig. 3 for a typical month (February 2014), along with the RT, PVT and
189 LRT marked in the figure. In general, the RT agreed well with both the LRT and PVT
190 in height, and most of the RT exhibit a slightly higher altitude. However, the differences
191 between the RT and LRT are sometimes large (reach to $\sim 1-2$ km) especially when the
192 RT experience rapid change. Regardless of the background synoptic condition, the
193 difference in the definitions themselves is to a large degree the main contributing factor
194 for the large difference between the RT and LRT. For example, a second layer with
195 significant enhanced echo power is observed above the radar-derived RT for the cases
196 on 4 and 5 February 2012 (Fig.3a). According to the definitions, the RT well defined as
197 the first layer with echo enhanced and the LRT matched the second layer, similar to that
198 observed by Yamamoto et al., (2003) and Fukao et al., (2003). It is of note that the RT
199 well separates the troposphere characterized by low aspect sensitivity from the lower-

200 stratosphere characterized by high aspect sensitivity (Fig.3b).

201 **3.2. Comparisons between different definitions**

202 To further quantify the consistency and difference in altitude between different
203 tropopause definitions, a detailed comparison is carried out in this section. The seasonal
204 scatterplots for RT versus LRT and the histogram distribution of altitude differences
205 between the RT and LRT are illustrated in Fig. 4, during the period November 2011-
206 May 2017. A total of 2411 data pairs are obtained for comparison. Among them, the
207 number of data pairs is 845 for DJF (winter), 721 for MAM (spring), 321 for JJA
208 (summer), and 524 for SON (autumn). Comparisons have shown a good consistency
209 throughout the seasons and most of the RTs exhibit a slightly higher than the LRTs. The
210 correlation coefficient is 0.74, 0.80, 0.82, and 0.78 for DJF, MAM, JJA, and SON,
211 respectively. The mean and standard deviation difference (RT minus LRT) calculated
212 in DJF, MAM, JJA, and SON is (0.14 ± 0.75) , (0.26 ± 0.78) , (0.33 ± 0.56) , and
213 (0.12 ± 0.69) km, respectively. The proportion of the data pairs with differences <500 m
214 is reasonably good during four seasons and is 63%, 61%, 64%, and 67% for DJF, MAM,
215 JJA, and SON, respectively. ~~Fig. 4 explicitly indicates the good capability~~shows that
216 the RT derived by-of the Beijing MST radar to-determineagrees reasonably well with
217 the tropopause structure wellLRT throughout the seasons.

218 To examine the potential role of the sharpness, Fig. 5a and Fig. 5b show the
219 histogram distribution of the tropopause sharpness along with the probability density
220 curve for data pairs with difference (absolute values of RT minus LRT) <0.5 km and >1
221 km respectively. What is apparent is that most data pairs of Fig. 5a are located to the

222 right (higher sharpness values, with the peak of ~ 7.06 K/km) and of Fig. 5b are to the
223 left (lower sharpness values, with the peak of ~ 6.35 K/km). No matter whether this
224 distribution feature is associated with the cyclonic-anticyclonic systems (e.g. Randel et
225 al., 2007; Randel and Wu, 2010), the results more or less demonstrate that the larger
226 (weaker) tropopause sharpness contribute to lower (higher) difference between the RT
227 and LRT. From the perspective of seasonal statistics, the tropopause sharpness over
228 Beijing station shows similar distribution characteristics throughout the seasons (not
229 shown), which is different from that in polar regions where the sharpness is significantly
230 higher during summer than during winter (Zänagl and Hoinka, 2001).

231 The seasonal scatterplots and height difference distribution between the RT and
232 PVT are illustrated and quantified in Fig. 6. The total number of comparing data pairs
233 for winter, spring, summer, and autumn is 1422, 1260, 791, and 1145, respectively.
234 During winter and spring (Fig. 6a and 6b), the RTs agree reasonably well with the PVTs
235 with the correlation coefficient of 0.72 and 0.76 and the mean difference (RT minus
236 PVT) of $(0.55 \pm 0.84$ km) and $(1 \pm 0.89$ km), respectively. In contrast, the consistency
237 for summer and autumn (Fig. 6c and 6d) is relatively bad and with correlation
238 coefficient of 0.33 and 0.47 and mean difference of $(0.80 \pm 1.39$ km) and $(0.75 \pm 1.23$
239 km), respectively. Especially for summer, the proportion of the comparing data pairs
240 with difference < 0.5 km is only 10.6% (84). In autumn, need to note that most data pairs
241 with poor consistency is sampled during early autumn.

242 3.3. Observational characteristics in the vicinity of ~~the~~ tropopause

243 Measurements of radar middle mode are used for examining the horizontal wind,

244 return power, and effective wind data acquisition rate within 5-6 km of the tropopause
245 (upper troposphere and lower stratosphere). Left panels of Fig. 7 show the vertical
246 scatterplots of the static stability (represented by the buoyancy frequency squared) as a
247 function of height relative to the LRT and the right panels show the radar echo power
248 as a function of height relative to the RT, during two specific years 2012-2013 for
249 extended winter NDJFM and summer MJJAS seasons. Mean and standard deviations
250 are also plotted in each panel of Fig. 7. As expected, Results-results clearly demonstrate
251 theshow sudden jump in static stability and rapid increase in echo-radar power upon
252 near the corresponding-tropopause layer. The degree of sudden increasevariation in
253 echo power is more gradual than that in static stability. TThe amplitude of both the jump
254 and the sudden increase in radar power experienced a slightly larger during NDJFM
255 than that during MJJAS (red lines of right panels). Another interesting feature in the
256 lower-stratosphere is that both the static stability and radar power points show less
257 disperse during NDJFM than that during MJJAS.

258 Fig. 8 shows the profiles of mean radar effective wind data acquisition rate for low
259 and middle modes during November 2011-May 2017. Clearly, both Here, the “effective
260 data” of one specific range gate requires at least three non-coplanar beams have
261 received backscattered echoes, by which 3-dimensional wind can be derived. The mean
262 data-acquisition-rate pprofiles both exhibit an obvious inversion layer (i.e.a sudden
263 increase significantly with height) near the tropopause, with the first peak located ~1
264 km higher above the mean tropopause height. Note that the second inversion in middle
265 mode profile that occurred near 16 km is associated with the second tropopause. As

266 limited by the highest detectable altitude (the data acquisition rate decreased to lower
267 than 20% at ~16 km), the profile in low mode shows little evidence of second inversion.

268 Fig. 9 shows time-height intensity plot of the monthly mean radar-derived
269 horizontal wind (from middle mode) during November 2011-May 2017, together with
270 the monthly mean location of RT and LRT. One pixel grid denotes 1 month×0.6 km.
271 The monthly mean RT and LRT agreed well with each other in height, within 400 m in
272 August and September and even lower in other months of about within 200 m. They
273 both exhibit a clear seasonal variation, with maximum in early autumn of ~11.6 km and
274 minimum in early spring of ~10.3 km. The monthly mean wind jet varies with season,
275 with the thinnest thickness and lowest strength in summer. The mean tropopause height
276 appears to correspond to the lower boundary location of peak wind layer. The error bars
277 of both the RT and LRT help to illustrate that the tropopauses changes by larger
278 amplitude in winter and June than that in other months.

279 **3.4. Periodogram analysis of the radar tropopause**

280 High temporal resolution detection of tropopause by VHF radar have allowed us
281 to investigate the diurnal or semidiurnal variability of the tropopause. Atmospheric tides
282 are well known global oscillations contributing to the diurnal variation in temperature
283 and background winds, which in turn modulate the tropopause height. With the absence
284 of high resolution temperature measurements, radar-derived winds are combined used
285 to represent the evidence of diurnal or semidiurnal variation in tropopause height that
286 modulated by tidal. The frequency power spectrum of the RT height, zonal and
287 meridional wind, calculated by means of Lomb-Scargle method (Press and Rybicki,

288 1989), is illustrated in Fig. 10 for two typical months: May 2015 and December 2016.
289 The choice of Lomb-Scargle algorithm is due to the presence of data gaps (~2 days per
290 week, especially during 2012-2013). The dominant ~24 h periodicity in RT height,
291 zonal and meridional wind is obvious for both months. The evidence of ~12 h period in
292 all three parameters is distinct for May 2015 (Fig. 10a), although the power is relatively
293 weaker. Through the analysis for each individual month, we found that the semidiurnal
294 component in the three parameters is generally and occasionally observed in summer
295 and later spring during our experimental period. The characteristics of the diurnal
296 variation of the RT height can be represented better in Fig. 11, which shows the mean
297 Lomb-Scargle power spectrum of the RT as a function month during November 2011-
298 May 2017. As compared with other months, the dominant diurnal periodicity is less
299 evident in April. We need to clarify that atmospheric tides are of course not the only
300 source of the diurnal variation in tropopause height, diurnal convective activities
301 (Yamamoto et al., 2003) might also be an important cause. Here will not be detailly
302 discussed.

303

304 **4. Discussion**

305 As for the radar echo power definition, the RT estimation sometimes will fail due
306 to the system problems, even if the thermal tropopause is well defined (Hall et al., 2009).
307 Apart from the system problems, the following two conditions are primarily responsible
308 for the failure (or difficulty) of both the radar and thermal definitions over the radar site
309 latitude (~40° N). Firstly, the temperature sometimes continue to decrease upon into the

310 lower stratosphere (below 16 km) in summer and early autumn, leading to the
311 failure/difficulty of both the radar and thermal definitions (a typical case as shown in
312 Fig. 12a). Need to note that the temperature inversion layer occurred at ~16 km in
313 summer or early autumn is the second tropopause with characteristics of Tropics (Pan
314 et al., 2004; Randel et al., 2007). Secondly, some specific meteorological processes can
315 lead to the ambiguities and indefiniteness in thermal and radar definitions, such as
316 fronts, cyclones or typhoons, and folding (e.g. Nastrom et al., 1989; May et al., 1991;
317 Roettger, 2001; Alexander et al., 2013). Such ambiguities often result in large difference
318 in altitude between the RT and LRT. ~~Especially~~ In addition, when multiple temperature
319 inversion layers occurred (below 16 km), the RT generally matched the lower part and
320 LRT often matched the upper part (e.g. Yamamoto et al., 2003; Fukao et al., 2003), such
321 as the double layers of enhanced echo power shown in Fig. 3 on 4 and 5 February 2012.
322 Apart from the two situations above, there is another condition that is commonly
323 responsible for the failure of thermal definition in summer and early autumn. As the
324 typical case shown in Fig. 12b, a significant inversion in temperature (at ~12 km) is
325 recorded from the radiosonde profile, but this inversion layer is too thin and weak to
326 meet the WMO criterion that thermal definition required. Whereas, the apparent
327 enhancement in radar echo power corresponding to such inversion layer is strong
328 enough to well define the RT. Need to highlight again that the temperature inversion
329 ~~layer located near ~16 km (the second tropopause) that occurred near ~16 km is the~~
330 ~~second tropopause (is not considered here the focus of this paper). The conditions~~
331 ~~mentioned above are the main reasons for fewer comparison data pairs in summer than~~

332 ~~that in other seasons (Fig. 4e and Fig. 6e).~~

333 Pan et al., (2004) have reported that the difference between the LRT and PVT are
334 more distinct in the vicinity of subtropical jet. In the northern hemisphere, the axis of
335 the subtropical jet is situated near $\sim 30^\circ\text{N}$ in spring and winter, whereas in summer and
336 early autumn the subtropical jet shifts northward to $\sim 40^\circ\text{N}$ (see Fig. 4 in Ding and Wang,
337 2006). We preliminary considered that the bad consistency between the RT and PVT in
338 summer and early autumn (Fig. 6c and 6d) is most likely associated with the subtropical
339 jet shifting poleward to $\sim 40^\circ\text{N}$. ~~The existing cyclones or anticyclones in the upper-~~
340 ~~troposphere (Wirth, 2000), of course, may also be an important influence factor for~~
341 ~~the cause of the significant asymmetric differences (most of the scattered points deviate~~
342 ~~significantly from the 1:1 line).~~ ~~(The asymmetric differences, that is scattered points~~
343 ~~deviate significantly from the 1:1 line and PVT located below the RT in most cases~~
344 ~~most of the RT are located higher than the 2PVU tropopause height, as shown in Fig. 6e),~~
345 ~~suggest that the 2PVU surface is not the best measure of a dynamical tropopause over~~
346 ~~Beijing during summer-time.~~ More detailed discussion about the striking asymmetric
347 differences in height between LRT and PVT can be seen in Wirth (2001) ~~and will not~~
348 ~~be given here.~~ Anyway, we need to be careful when using the 2PVU dynamical
349 definition to define the tropopause over radar site latitude $\sim 40^\circ\text{N}$, especially in summer.

350 About the characteristics of tropopause and the comparison between different
351 definitions, there are many differences between mid-latitude and polar regions. In mid-
352 latitude ($\sim 40^\circ\text{N}$), our results show that: (1) the agreement between RT and LRT is
353 similar good throughout the seasons; (2) RTs are generally located higher than the LRT;

354 (3) the thermal definition sometimes fail in summer and early autumn; (4) the
355 agreement between the RT/LRT and PVT in summer is poor. Whereas, in contrast,
356 previous researches about the tropopause over polar regions showed that (Wirth, 2000;
357 [Alexander et al., 2012](#) [Alexander et al., 2013](#)): (1) the difference between the RT and
358 LRT is larger during winter than that during summer; (2) RTs are generally located
359 lower than the LRT; (3) the thermal definition sometimes fail in winter and spring; (4)
360 comparison between the RT and PVT showed the similar good agreement during both
361 summer and winter.

362 Over a polar latitude station, the seasonal characteristics of the diurnal oscillation
363 in tropopause height were investigated using 5 years of SOUSY VHF radar
364 measurements (Hall, 2013b). The sunlight variability in polar regions is different from
365 that in other latitudes of the world. Different sunlight variation actually will lead to
366 difference in atmospheric tides, and then would result in different diurnal variation in
367 tropopause height. Here we found that the diurnal oscillation of RT height at Xianghe
368 is ubiquitous and obvious throughout the seasons except for April (Fig. 11). Whereas at
369 polar latitude and in months of November to February when there is no sunlight, Hall
370 (2013b) observed little evidence of 24 h diurnal variability in RT height.

371

372 **5. Conclusions**

373 In this paper, we present the high resolution structure and variability of the
374 tropopause in Xianghe, China (39.75° N, 116.96° E), based on the Beijing MST radar
375 vertical beam echo power data collected during the period November 2011-May 2017.

376 Fine-scale structure of the RT is well determined with a high temporal resolution of 0.5
377 h. Comparison results have shown good agreement in altitude between the RT and LRT,
378 with a correlation coefficient of ≥ 0.74 for the four seasons. Higher tropopause
379 sharpness seems to contribute lower difference between the RT and LRT in altitude and
380 weaker sharpness appears responsible for higher difference. The agreement between
381 the RT and PVT is relatively well in winter and spring with correlation coefficient of
382 0.72 and 0.76 respectively, but poor during summer with a correlation coefficient of
383 only 0.33. We initially suggested that the poor consistency between RT and PVT is
384 associated with the subtropical jet shifting poleward to $\sim 40^\circ\text{N}$.

385 As expected, the sudden jump in static stability (represented by the buoyancy
386 frequency squared) and the rapid increase in radar echo power upon the tropopause
387 layer are clearly observed. Upon the tropopause layer, A significant inversion
388 (increasing with height) sudden increase in effective radar data acquisition rate is also
389 observed upon the tropopause layer. Both the monthly mean RT and LRT height have
390 shown a clear annual cycle. The variability and oscillation of RT height with diurnal or
391 lower timescales is presented. Obvious diurnal variation in tropopause height, zonal
392 wind, and meridional wind is generally observed throughout the seasons, indicating the
393 modulation most likely from the atmospheric tides. The semidiurnal variation in RT
394 height is not so obvious and commonly observed occasionally in summer and late
395 spring.

396

397 **Acknowledgment**

398 This work is funded by National Natural Science Foundation of China (NSFC grants
399 No. 41474132 and 41722404). We acknowledge the Chinese Meridian Project for
400 providing the MST radar data. The authors sincerely acknowledge the ECMWF for
401 providing global reanalysis data. The MST radar data for this paper are available at
402 Data Centre for Meridian Space Weather Monitoring Project (<http://159.226.22.74/>).
403 The radiosonde data are publicly available from the NOAA/ESRL Database at
404 <https://ruc.noaa.gov/raobs/>.

405

406 **References**

407 Alexander, S.P., Murphy, D.J., and Klekociuk, A.R.: High resolution VHF radar
408 measurements of tropopause structure and variability at Davis, Antarctica (69° S,
409 78° E), Atmos. Chem. Phys., 13, 3121-3132, 2013.~~Alexander, S. P., Murphy, D. J.,~~
410 ~~and Klekociuk, A. R.: High resolution VHF radar measurements of tropopause~~
411 ~~structure and variability at Davis, Antarctica (69° S, 78° E). Atmospheric~~
412 ~~Chemistry and Physics, 12(10), 26173-26205, 2012.~~

413 Angell, J. K., and Korshover, J.: Quasi-biennial and long-term fluctuations in
414 tropopause pressure and temperature, and the relation to stratospheric water vapor
415 content. Monthly Weather Review, 102(1), 29-34, 2009.

416 Appenzeller, C., Holton, J. R., and Rosenlof, K. H.: Seasonal Variation of Mass
417 Transport Across the Tropopause. Journal of Geophysical Research, 101(D10),
418 15071-15078, 1996.

419 Añel, J. A., J. C. Antuña, L. de la Torre, R. Nieto, and Gimeno L.: Changes in

420 tropopause height for the Eurasian region determined from CARDS radiosonde
421 data. *Naturwissenschaften*, 93, 603–609, doi:10.1007/s00114-006-0147-5, 2006.

422 Bethan, S., Vaughan, G., and Reid, S. J.: A comparison of ozone and thermal tropopause
423 heights and the impact of tropopause definition on quantifying the ozone content
424 of the troposphere. *Quarterly Journal of the Royal Meteorological Society*,
425 122(532), 929-944, 1996.

426 Baray, J., Daniel, V., Ancellet, G., and Legras, B.: Planetary-scale tropopause folds in
427 the southern subtropics. *Geophysical Research Letters*, 27(3), 353-356, 2000.

428 Chen, F. L., Chen, G., Shi, C. H., Tian, Y. F., Zhang, S. D., and Huang, K. M.: Strong
429 downdrafts preceding rapid tropopause ascent and their potential to identify cross-
430 tropopause stratospheric intrusions, *Annales Geophysicae*, 36(5), 1403-1417,
431 2018.

432 Chen, G., Cui, X., Chen, F., Zhao, Z., Wang, Y., Yao, Q., and Gong, W.: MST Radars
433 of Chinese Meridian Project: System Description and Atmospheric Wind
434 Measurement. *IEEE Transactions on Geoscience and Remote Sensing*, 54(8),
435 4513-4523, 2016.

436 Das, S. S., Jain, A. R., Kumar, K. K., and Rao, D. N.: Diurnal variability of the tropical
437 tropopause: Significance of VHF radar measurements. *Radio Science*, 43(6), 1-14,
438 doi:10.1029/2008RS003824, 2008.

439 Dee, D. P., Uppala, S. M., Simmons, A. J., Berrisford, P., Poli, P., Kobayashi, S. et al.:
440 The ERA-Interim reanalysis: configuration and performance of the data
441 assimilation system. *Quarterly Journal of the Royal Meteorological Society*,

442 137(656), 553-597, 2011.

443 Ding, A., and Wang, T.: Influence of stratosphere-to-troposphere exchange on the
444 seasonal cycle of surface ozone at Mount Waliguan in western China. *Geophysical*
445 *Research Letters*, 33(3), 233-252, doi:10.1029/2005GL024760, 2006.

446 Fukao, S., H. Hashiguchi, M. Yamamoto, T. Tsuda, T. Nakamura, M. K. Yamamoto,
447 T. Sato, M. Hagio, and Y. Yabugaki: Equatorial Atmosphere Radar (EAR):
448 System description and first results. *Radio Science*, 38(3), 1053, 2003.

449 Gage, K. S., and Green, J. L.: An objective method for the determination of tropopause
450 height from VHF radar observations. *Journal of Applied Meteorology*, 21(21),
451 1150-1154, 1982.

452 Gage, K. S., and Green, J. L.: Tropopause Detection by Partial Specular Reflection with
453 Very-High-Frequency Radar. *Science*, 203(4386), 1238-1240, 1979.

454 Gettelman, A., P. Hoor, L. L. Pan, W. J. Randel, M. I. Hegglin, and T. Birner: The
455 extratropical upper troposphere and lower stratosphere, *Reviews of Geophysics*,
456 49(3), RG3003, doi: 10.1029/2011RG000355, 2011.

457 Hermawan, E., Tsuda, T., and Adachi, T.: MU radar observations of tropopause
458 variations by using clear air echo characteristics. *Earth, Planets and Space*, 50(4),
459 361-370, 1998.

460 Hall, C.: The radar tropopause above Svalbard 2008–2012: Characteristics at various
461 timescales. *Journal of Geophysical Research*, 118(6), 2600-2608, 2013a.

462 Hall, C.: The radar tropopause at 78°N, 16°E: Characteristics of diurnal variation.
463 *Journal of Geophysical Research*, 118(12), 6354-6359, doi:10.1002/jgrd.50560,

464 2013b.

465 Hall, C. M., Röttger, J., Kuyeng, K., Sigernes, F., Claes, S., and Chau, J. L.: Tropopause
466 altitude detection at 78°N, 16°E, 2008: First results of the refurbished SOUSY
467 radar. *Radio Science*, 44(5), 1-12, doi:10.1029/2009RS004144, 2009.

468 Hoinka, K. P.: Statistics of the Global Tropopause Pressure. *Monthly Weather Review*,
469 126(12), 3303-3325, 1998.

470 Hoskins, B. J., McIntyre, M. E., and Robertson, A. W.: On the use and significance of
471 isentropic potential vorticity maps. *Quarterly Journal of the Royal Meteorological
472 Society*, 111(470), 877-946, 2007.

473 Huang, C., Zhang, S. D., Zhou, Q. H., Yi, F., Huang, K., Gong, Y., Zhang, Y., and Gan,
474 Q.: WHU VHF radar observations of the diurnal tide and its variability in the lower
475 atmosphere over Chongyang (114.14° E, 29.53° N), China. *Annales Geophysicae*,
476 33(7), 865-874, 2015.

477 Hoerling, M. P., Schaack, T. K., and Lenzen, A. J.: Global Objective Tropopause
478 Analysis. *Monthly Weather Review*, 119(8), 1816-1831, 1991.

479 Liu, Y., Xu, T., and Liu, J.: Characteristics of the seasonal variation of the global
480 tropopause revealed by cosmic/GPS data. *Advances in Space Research*, 54(11),
481 2274-2285, 2014.

482 May, P. T., Yamamoto, M., Fukao, S., Sato, T., Kato, S., and Tsuda, T.: Wind and
483 reflectivity fields around fronts observed with a VHF radar. *Radio Science*, 26(5),
484 1245-1249, 1991.

485 Nastrom, G. D., Green, J. L., Gage, K. S., and Peterson, M. R.: Tropopause Folding
486 and the Variability of the Tropopause Height as Seen by the Flatland VHF Radar.
487 *Journal of Applied Meteorology*, 28(12), 1271-1281, 1989.

488 Nielsen-Gammon, J. W.: A visualization of the global dynamic tropopause. *Bulletin of*
489 *the American Meteorological Society*, 82(6), 1151-1168, 2001.

490 Pan, L. L., Randel, W. J., Gary, B. L., Mahoney, M. J., and Hints, E. J.: Definitions
491 and sharpness of the extratropical tropopause: A trace gas perspective. *Journal of*
492 *Geophysical Research*, 109, D23103, doi:10.1029/2004JD004982, 2004.

493 Pan, L. L., W. J. Randel, J. C. Gille, W. D. Hall, B. Nardi, S. Massie, V. Yudin, R.
494 Khosravi, P. Konopka, and D. Tarasick: Tropospheric intrusions associated with
495 the secondary tropopause, *Journal of Geophysical Research*, 114, D10302, 2009.

496 Press, W. H., and Rybicki, G. B.: Fast algorithm for spectral analysis of unevenly
497 sampled data. *The Astrophysical Journal*, 338(1), 277-280, 1989.

498 Ravindrababu, S., Venkat Ratnam, M., Sunilkumar, S. V., Parameswaran, K., and
499 Krishna Murthy, B. V.: Detection of tropopause altitude using Indian MST radar
500 data and comparison with simultaneous radiosonde observations. *Journal of*
501 *Atmospheric and Solar-Terrestrial Physics*, 121(6), 679-687, 2014.

502 Randel, W. J., Wu, F., and Gaffen, D. J.: Interannual variability of the tropical
503 tropopause derived from radiosonde data and NCEP reanalyses. *Journal of*
504 *Geophysical Research Atmospheres*, 105(D12), 15509-15523, 2000.

505 Randel, W. J., Seidel, D. J., and Pan, L. L.: Observational characteristics of double
506 tropopauses. *Journal of Geophysical Research*, 112, D07309, 2007.

507 Randel, W. J., and Wu, F.: The Polar Summer Tropopause Inversion Layer. *Journal of*
508 *the Atmospheric Sciences*, 67(8), 2572-2581, 2010.

509 Randel, W. J., Wu, F., and Forster, P. M.: The extratropical tropopause inversion layer:
510 Global observations with GPS data, and a radiative forcing mechanism. *Journal of*
511 *the Atmospheric Sciences*, 64(12), 4489-4496, 2007.

512 Ramakrishnan, K. P.: Distortion of the tropopause due to meridional movements in the
513 sub-stratosphere. *Nature*, 132(3346), 932-932, 1933.

514 Roettger, J.: Observations of the polar d-region and the mesosphere with the Eiscat
515 Svalbard radar and the SOUSY Svalbard Radar (scientific paper). *Memoirs of*
516 *National Institute of Polar Research. Special Issue*, 54(94), 9-20, 2001.

517 Reed, R. J.: A study of a characteristic type of upper-level frontogenesis. *Journal of the*
518 *Atmospheric Sciences*, 12(3), 226-237, 1955.

519 Santer, B. D., Wehner, M. F., Wigley, T. M., Sausen, R., Meehl, G. A., Taylor, K. E.,
520 Ammann, C., Arblaster, J., Washington, W. M., Boyle, J. S., and Brüggemann, W.:
521 Contributions of anthropogenic and natural forcing to recent tropopause height
522 changes. *Science*, 301(5632), 479-483, 2003.

523 Santer, B. D., Sausen, R., Wigley, T. M., Boyle, J. S., Achutarao, K., Doutriaux, C.,
524 Hansen, J. E., Meehl, G. A., Roeckner, E., Ruedy, R., Schmidt, G., and Taylor, K.
525 E.: Behavior of tropopause height and atmospheric temperature in models,
526 reanalyses, and observations: Decadal changes. *Journal of Geophysical Research*,
527 108(D1), 4002, doi:10.1029/2002JD002258, 2003a.

528 Sausen, R., and Santer, B. D.: Use of Changes in Tropopause Height to Detect Human

529 Influences on Climate. Meteorologische Zeitschrift, 12(3), 131-136, 2003.

530 Schmidt, T., Heise, S., Wickert, J., Beyerle, G., & Reigber, C.: GPS radio occultation
531 with CHAMP and SAC-C: global monitoring of thermal tropopause parameters.
532 Atmospheric Chemistry and Physics, 5(6), 1473-1488, 2005.

533

534 Seidel, D. J., Ross, R. J., Angell, J. K., and Reid, G. C.: Climatological characteristics
535 of the tropical tropopause as revealed by radiosondes. Journal of Geophysical
536 Research, 106(D8), 7857-7878, 2001.

537 Son, S. W., Tandon, N. F., & Polvani, L. M.: The fine-scale structure of the global
538 tropopause derived from COSMIC GPS radio occultation measurements. Journal
539 of Geophysical Research: Atmospheres, 116(D20), 2011.

540 ~~Son, S., Tandon, N. F., and Polvani, L. M.: The fine-scale structure of the global~~
541 ~~tropopause derived from cosmic gps radio occultation measurements. Journal of~~
542 ~~Geophysical Research Atmospheres, 116, D20113, 2011.~~

543 Sprenger, M., Croci Maspoli, M., and Wernli, H.: Tropopause folds and cross-
544 tropopause exchange: a global investigation based upon ECMWF analyses for the
545 time period March 2000 to February 2001. Journal of Geophysical Research
546 Atmospheres, 108(12), 291-302, 2003.

547 Tian, Y., and Lu, D.: Comparison of Beijing MST Radar and Radiosonde Horizontal
548 Wind Measurements. Advances in Atmospheric Sciences, 34(1), 39-53. doi:
549 10.1007 / s00376-016-6129-4, 2017.

550 Vaughan, G., Howells, A., and Price, J. D.: Use of MST radars to probe the mesoscale

551 structure of the tropopause. *Tellus A*, 47(5), 759-765, 1995.

552 Wang, C.: Development of the Chinese meridian project. *Chinese Journal of Space*
553 *Science*, 30(4), 382–384, 2010.

554 [Wilcox L.J., Hoskins B.J., Shine K.P. 2012. A global blended tropopause based on ERA](#)
555 [data. Part I: Climatology. Q. J. R. Meteorol. Soc. 138: 561–575.](#)
556 [DOI:10.1002/qj.951.](#)

557 Wirth, V.: Thermal versus dynamical tropopause in upper-tropospheric balanced flow
558 anomalies. *Quarterly Journal of the Royal Meteorological Society*, 126(562), 299-
559 317, 2000.

560 Wirth, V.: Cyclone-anticyclone asymmetry concerning the height of the thermal and the
561 dynamical tropopause. *Journal of the Atmospheric Sciences*, 58(1), 26-37, 2001.

562 WMO: Definition of the tropopause. *WMO Bull.*, 6, 136, 1957.

563 Yamamoto, M., Oyamatsu, M., Horinouchi, T., Hashiguchi, H., and Fukao, S.: High
564 time resolution determination of the tropical tropopause by the Equatorial
565 Atmosphere Radar. *Geophysical Research Letters*, 30(21), 2094, 2003.

566 Zängl, G., and Hoinka, K. P.: The tropopause in the polar regions. *Journal of Climate*,
567 14(2001), 3117-3139, 2001.

568

569 **Table**

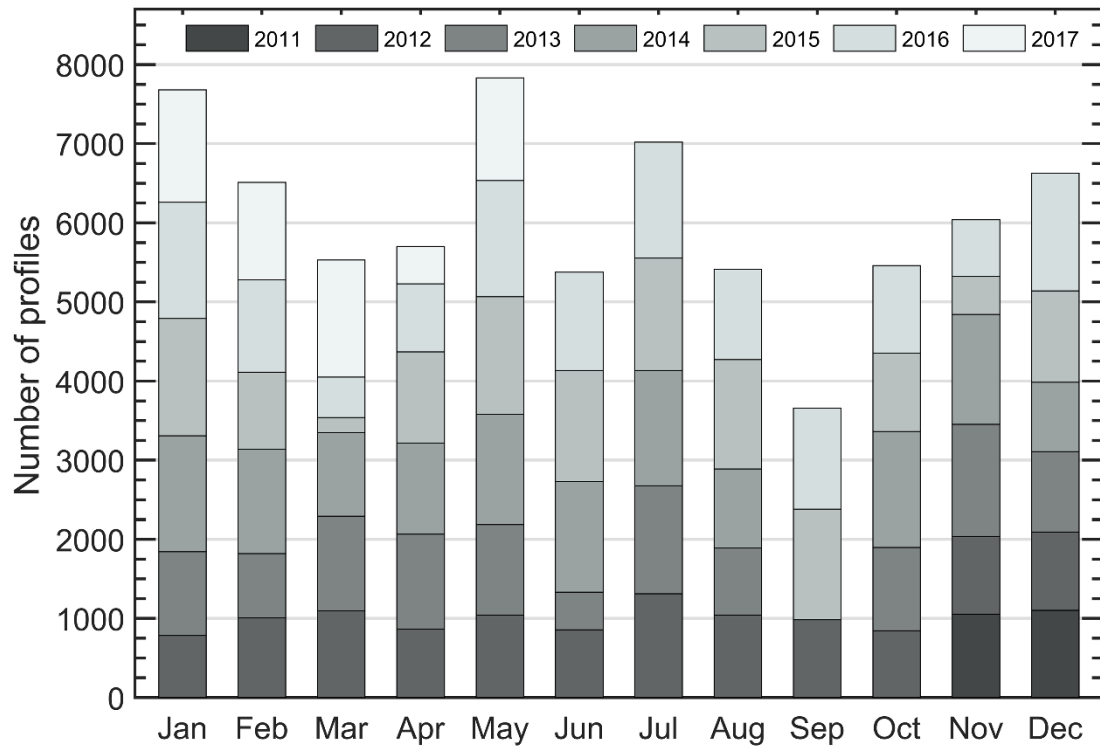
Radar parameter	Value
Transmitted frequency	50 MHz
Antenna array	24×24 3-element Yagi
Antenna gain	33 dB
Transmitter peak power	172 kW
Code	16-bit complementary
No. coherent integrations	128 (low mode)/64 (mid mode)
No. FFT points	256
No. spectral average	10
Pulse repetition period	160 (low mode)/320 (mid mode) μ s
Half power beam width	3.2°
Pulse length	1 (low mode)/4 (mid mode) μ s
Range resolution	150 (low mode)/600 (mid mode) m
Temporal resolution	30 min
Off-zenith angle	15°

570 **Table 1.** Routine operational parameters in low and middle mode for the Beijing MST

571 radar used in this study.

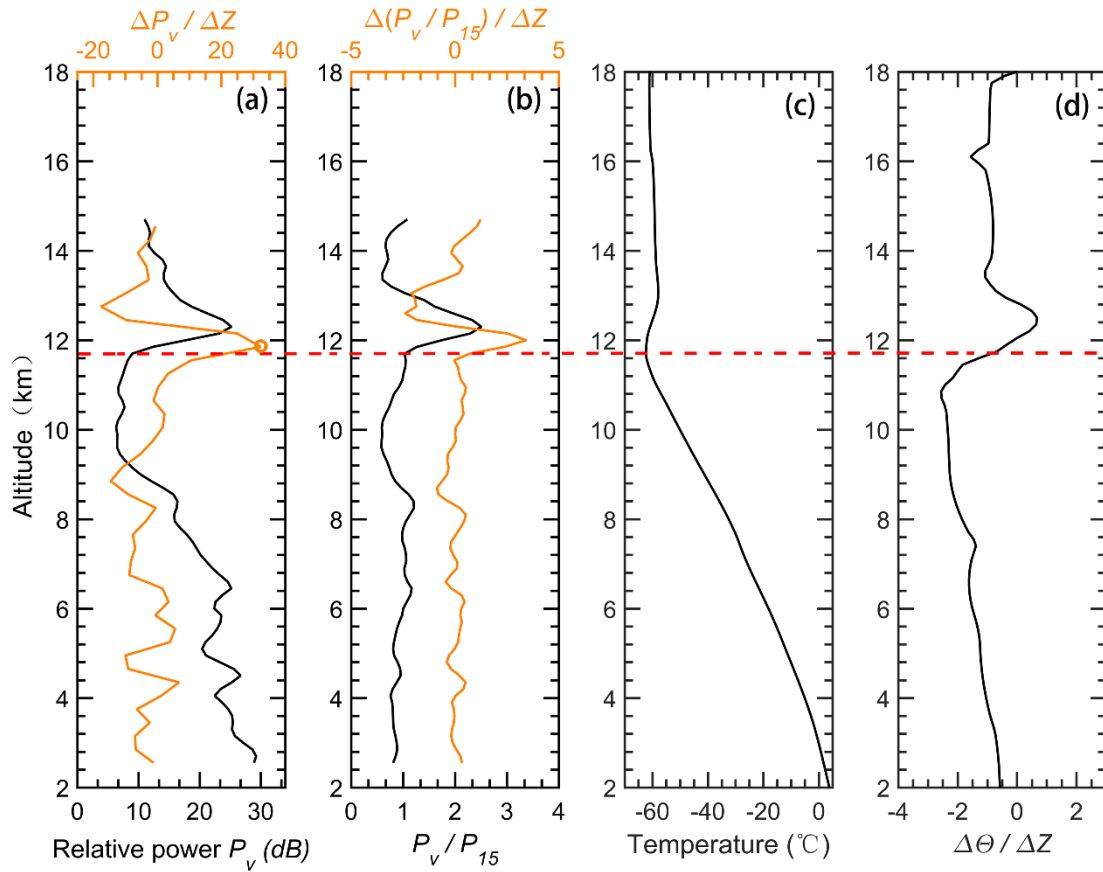
572

573 **Figures**



574

575 **Figure 1.** Distribution of the monthly total number of radar return echo power profiles
576 that available from vertical beam in low mode, collected for the period November 2011-
577 May 2017.

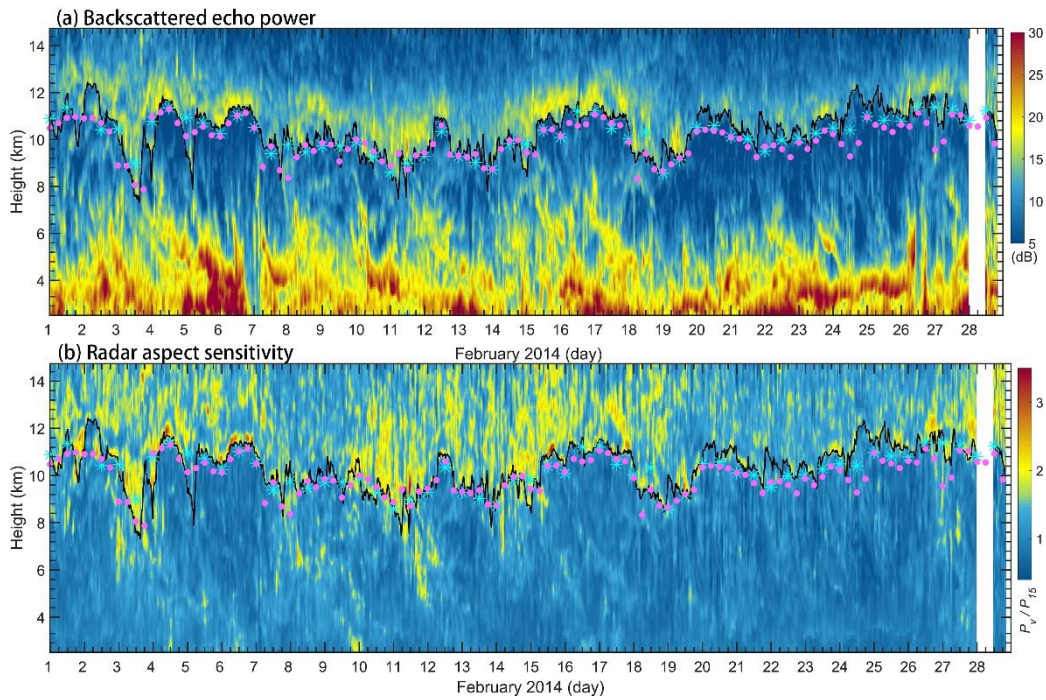


578

579 **Figure 2.** Example vertical profiles of (a) relative radar echo power (black line) along
 580 with its gradient variation (orange line), (b) radar aspect sensitivity (black line) along
 581 with its gradient variation (orange line), (c) radiosonde temperature and (d) potential
 582 temperature gradient on 00 UT 04 November 2011. The horizontal red dashed line
 583 marks the LRT height. The orange circle in Fig. 2a denotes the RT height.

584

585



586

587 **Figure 3.** Altitude-time intensity plot of (a) radar backscattered echo power and (b)

588 radar aspect sensitivity for February 2014. The tropopause determined based on the

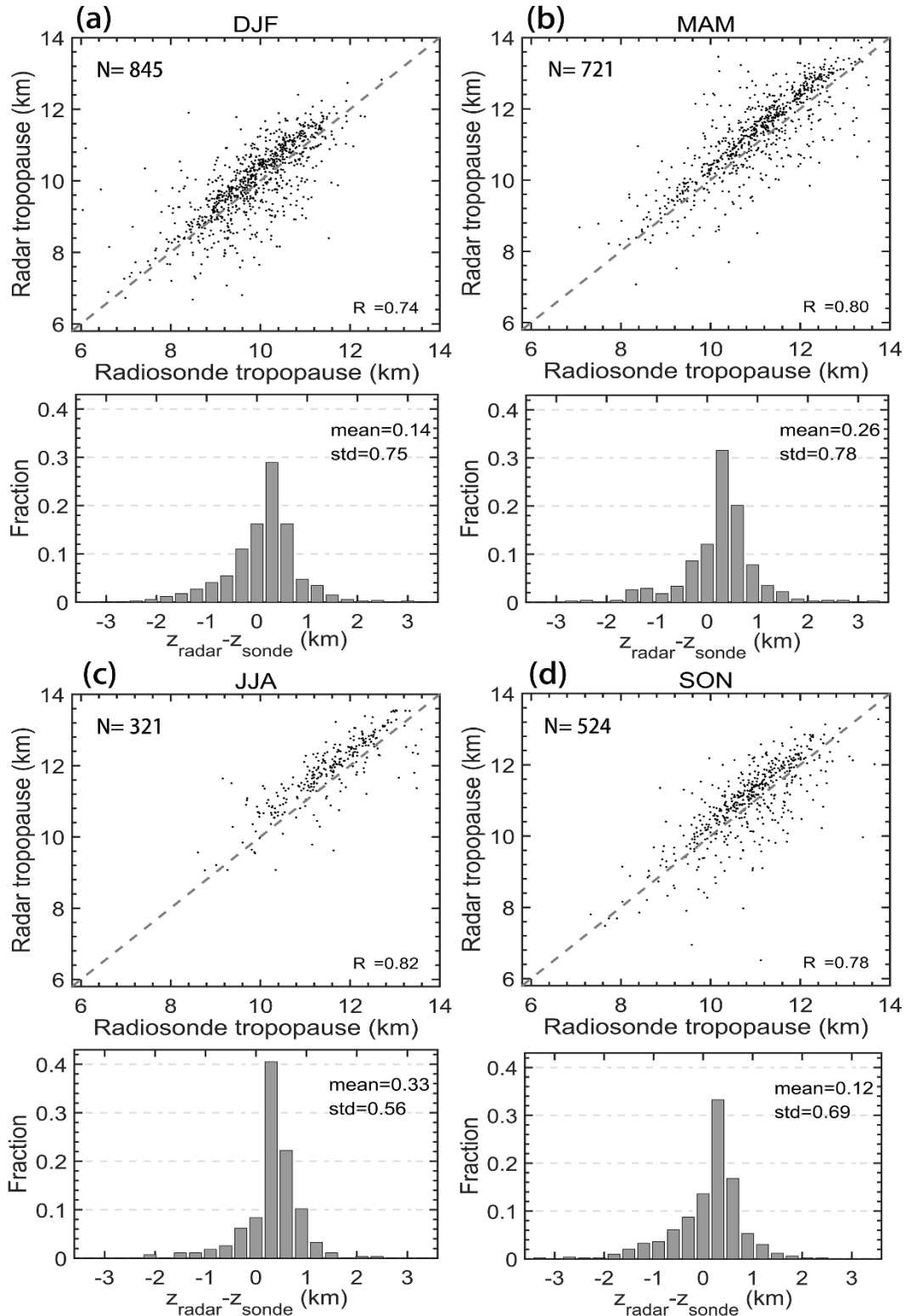
589 radar echo definition are shown as a black solid curve. The green-cyan asterisks ‘*’ and

590 pink dots indicate the location of the LRT derived from simultaneous twice daily

591 radiosonde data and the PVT from ECMWF ERA-Interim reanalysis, respectively.

592 White stripe indicates the time frame of radar missing data.

593



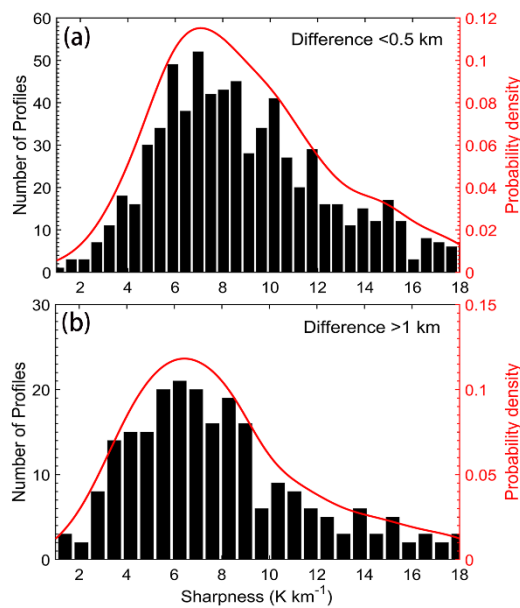
594

595 **Figure 4.** Seasonal scatterplots of the RT versus LRT and histogram distribution of
 596 altitude differences between the RT and the LRT, for (a) winter DJF, (b) spring MAM,
 597 (c) summer JJA, and (d) autumn SON, during the period November 2011-May 2017.

598 The positive values in the histogram indicate the RT locating at a higher level than the
 599 LRT. The grey dashed line shows the 1:1 line. Here, 'N', 'R²', 'mean', and 'std' indicate
 600 the sample numbers, correlation coefficient, mean difference, and standard deviation of
 601 the difference, respectively.

602

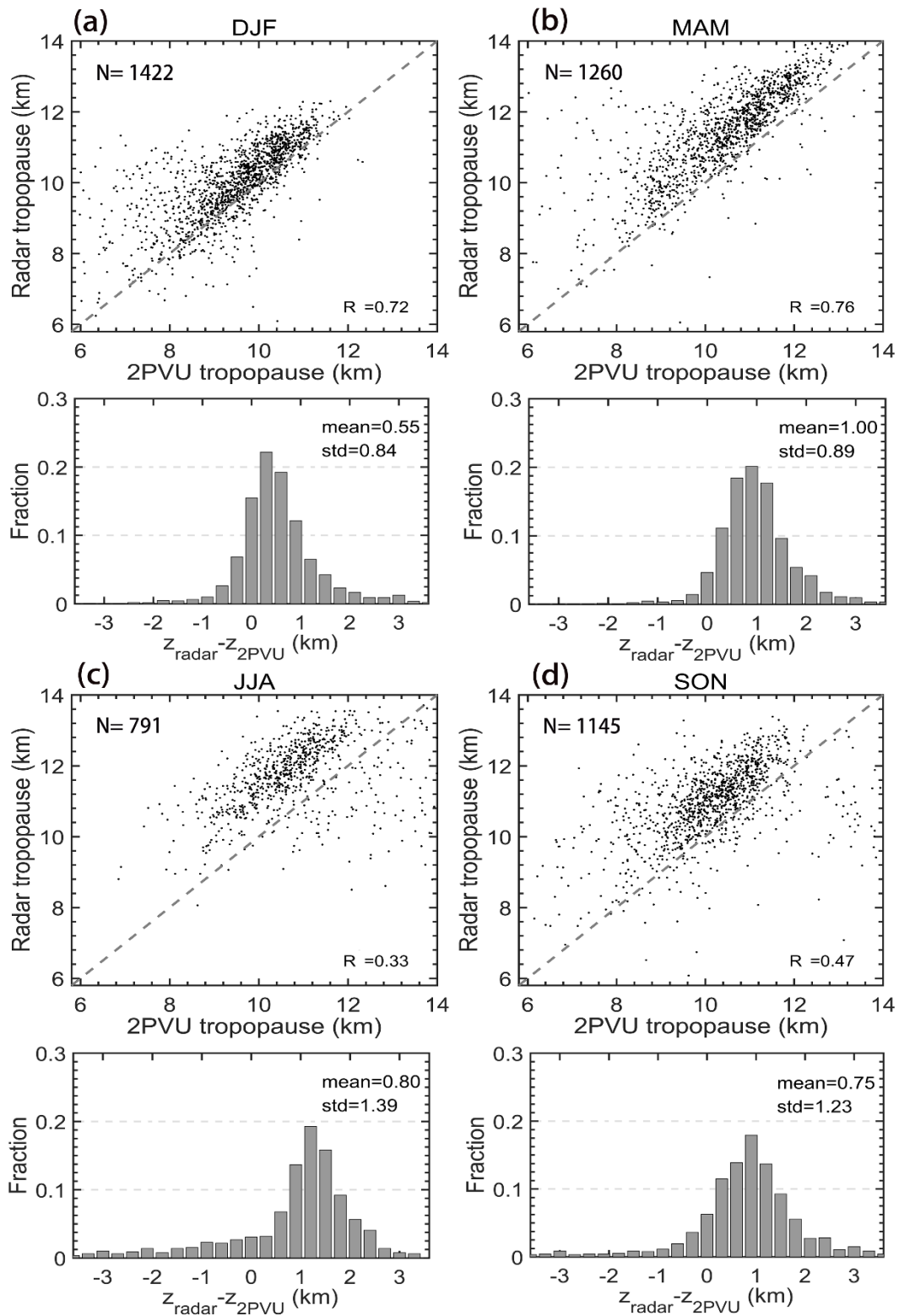
603



604

605 **Figure 5.** Histogram distribution of the tropopause sharpness for (a) difference <0.5
 606 km, and (b) >1 km respectively between the LRT and the RT.

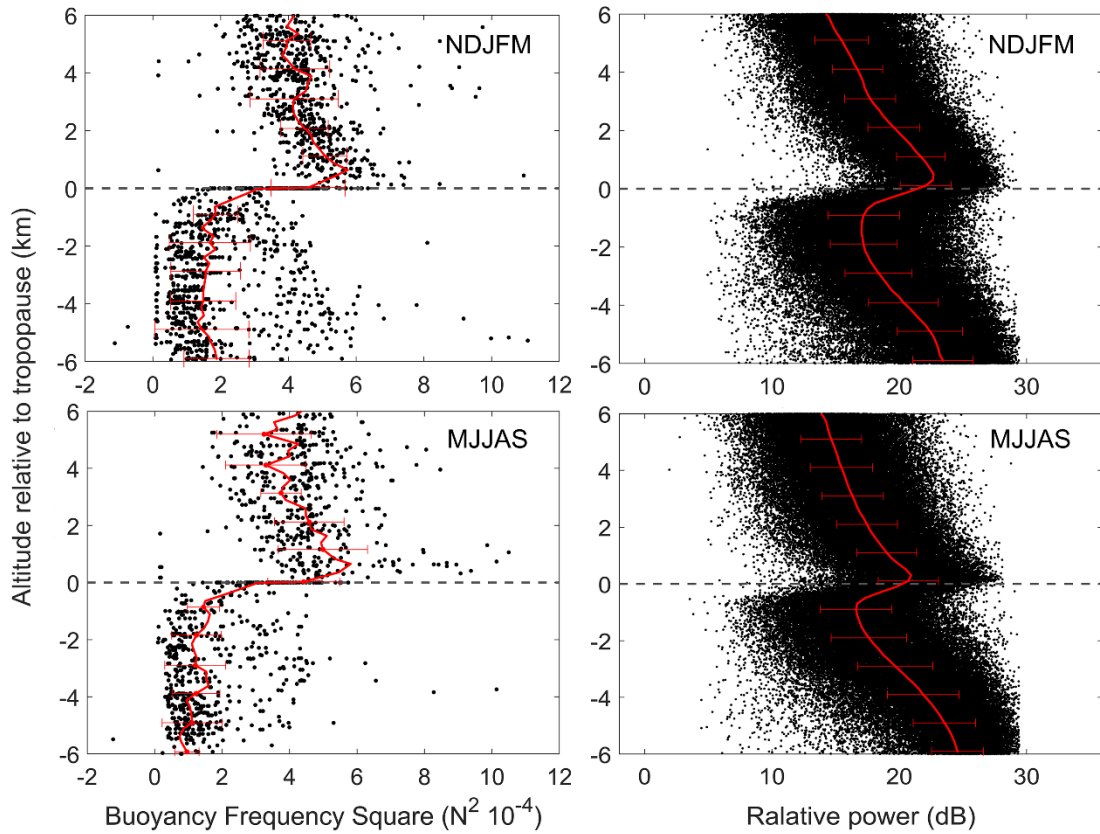
607



608

609 **Figure 6.** Same as figure 4, but for the comparison between the RT and the PVT.

610



611

612 **Figure 7.** Scatterplots of (left panels) static stability (N^2) and (right panels) radar

613 relative echo power as a function of altitude relative to the LRT (left panels) and RT

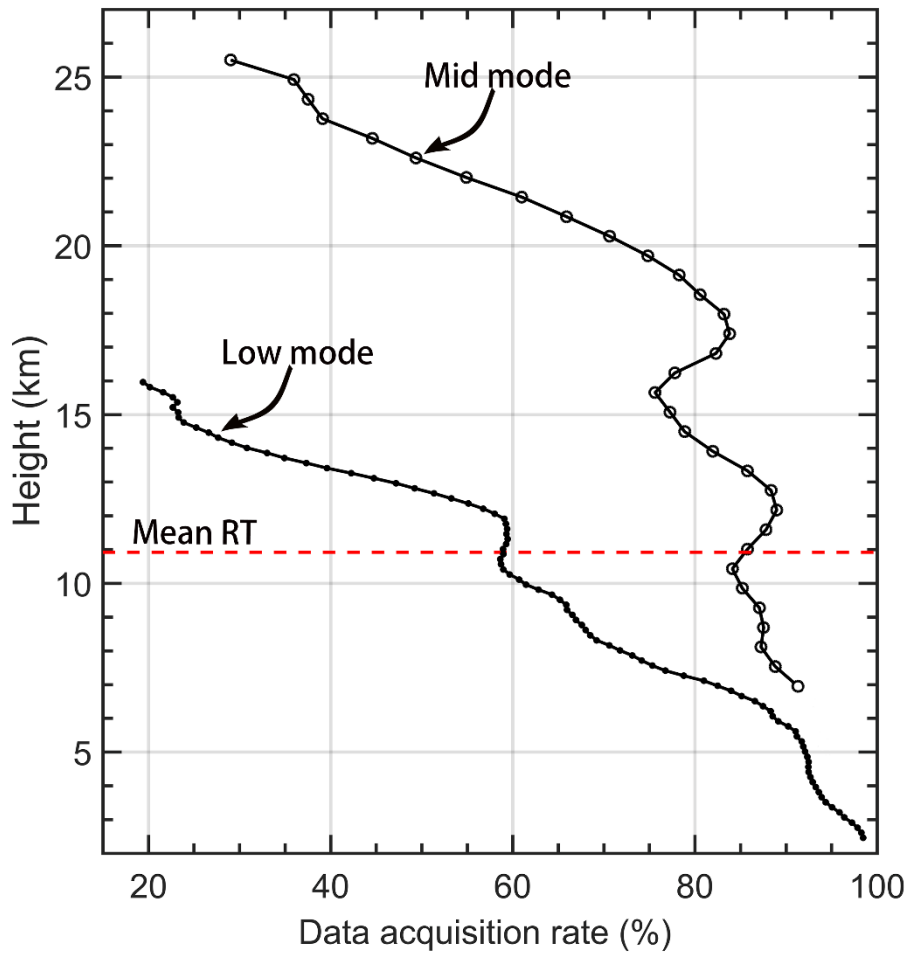
614 (right panels) for extended winter (NDJFM) and summer (MJJAS) seasons for two

615 specific years 2012-2013. Red lines in each panel denote the corresponding mean

616 profiles and the error bars indicate the standard deviations.

617

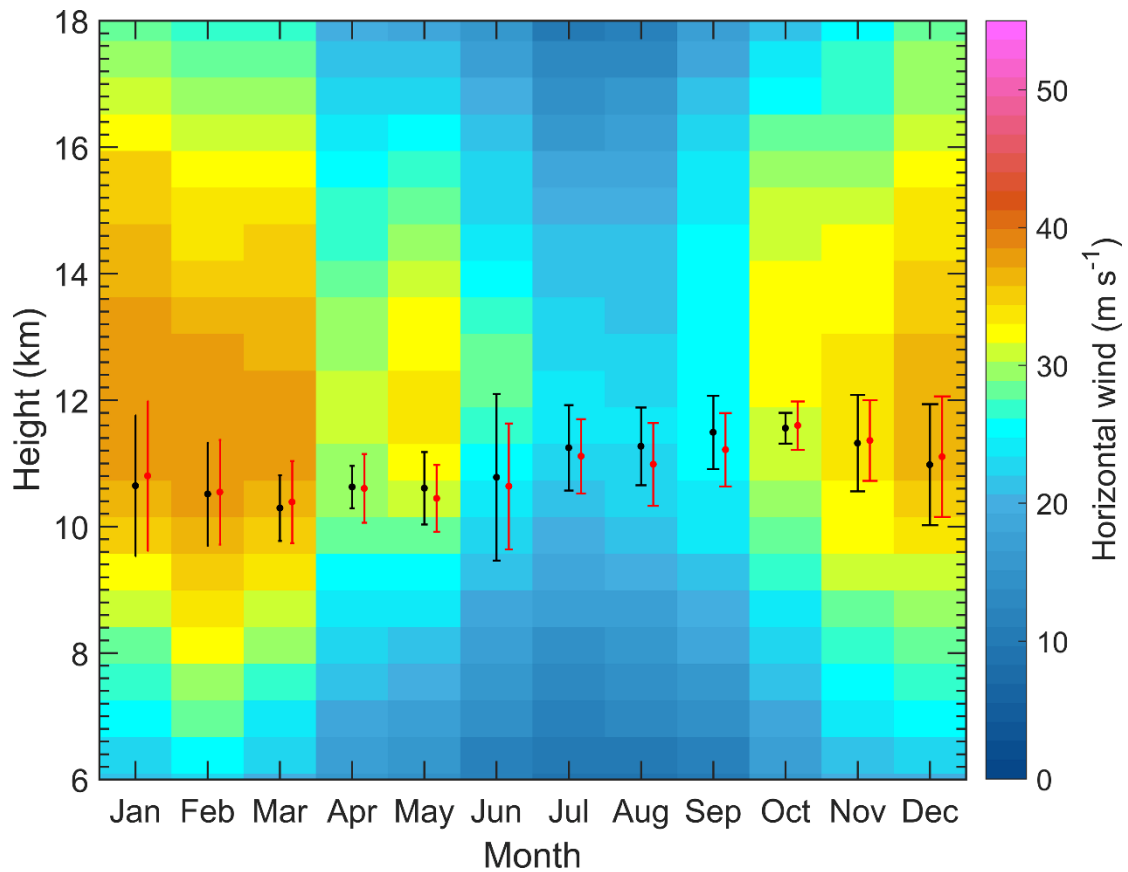
618



619

620 **Figure 8.** Vertical height profiles of the averaged effective radar wind data acquisition
 621 rate in low mode and middle mode during November 2011-May 2017. The red dashed
 622 line indicates the mean RT height.

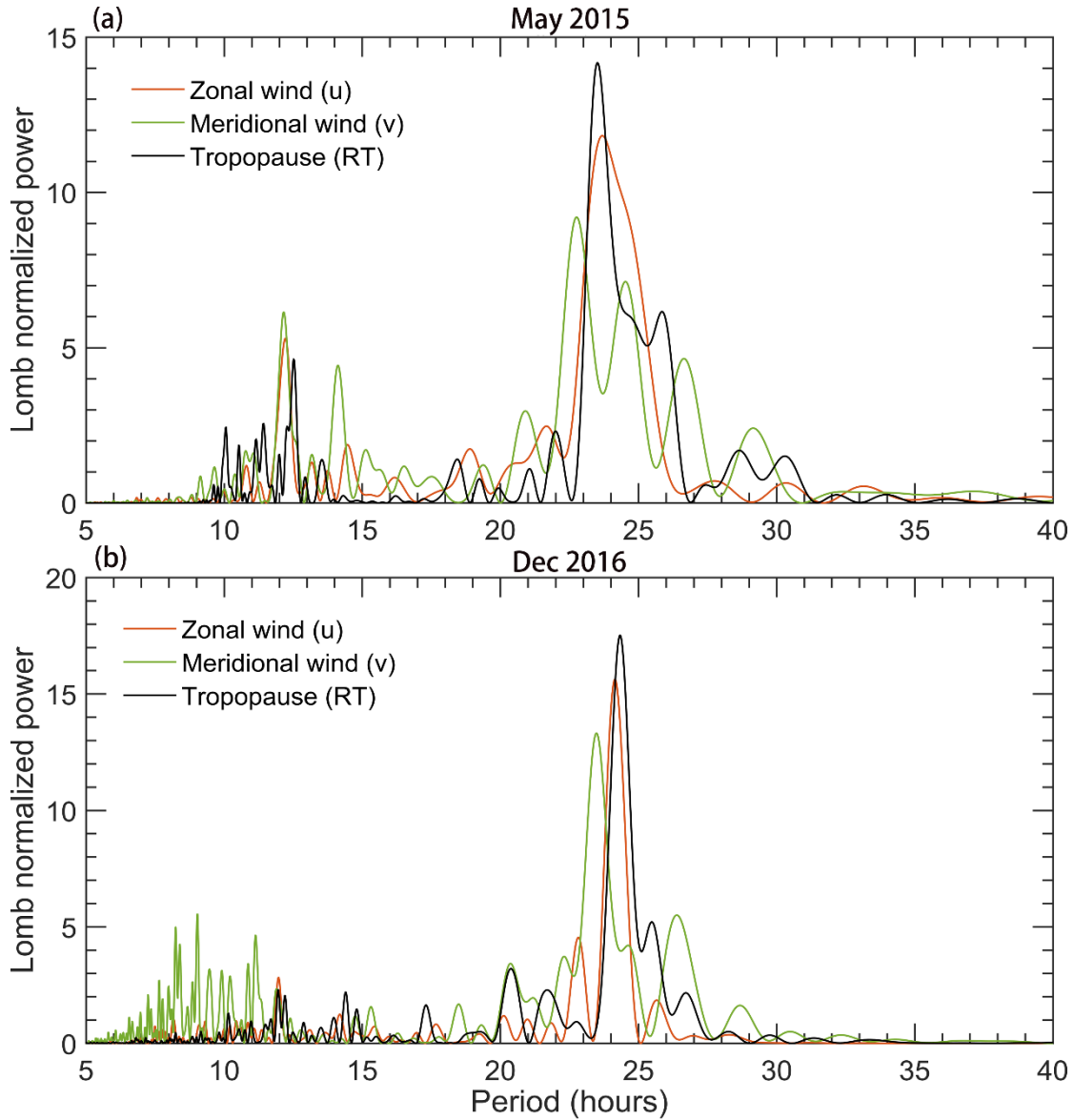
623



624

625 **Figure 9.** Height-time intensity map of monthly mean horizontal wind speed (shaded,
 626 m/s) derived from the middle mode of Beijing MST radar, during November 2011-May
 627 2017. Also shown is the monthly mean height of RT (black dots) and LRT (red dots,
 628 offset by +6 days) along with the vertical error bars representing the standard deviations.

629



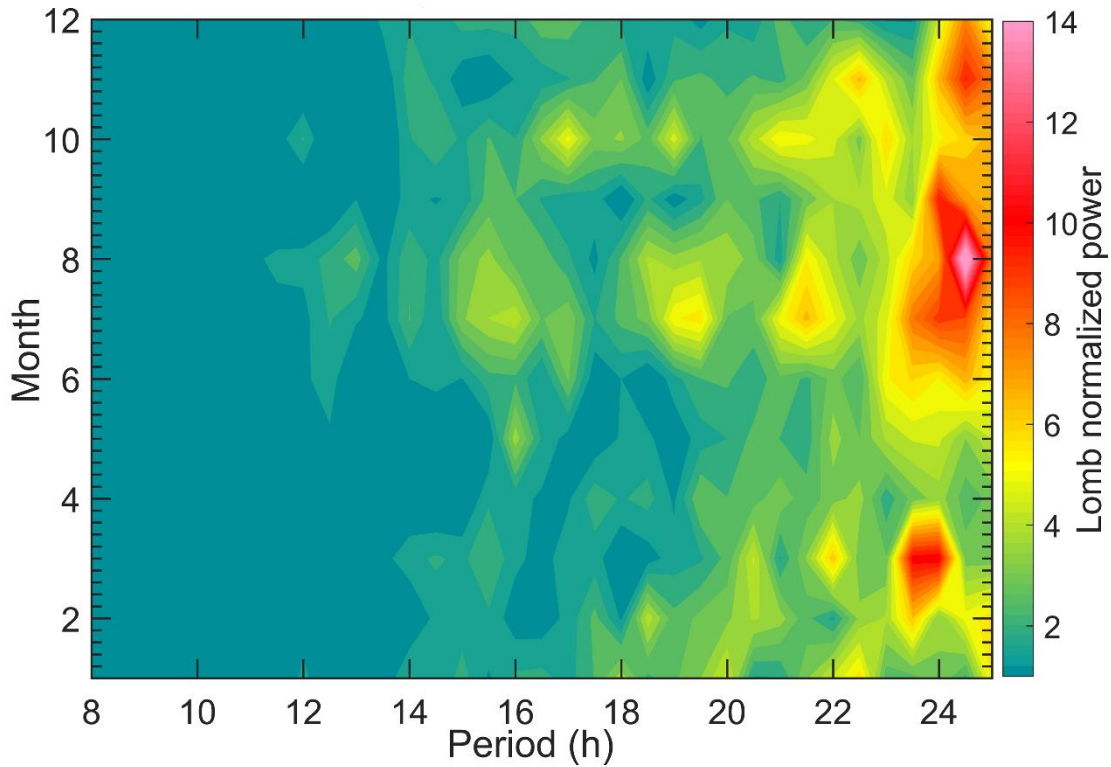
630

631 **Figure 10.** Lomb-Scargle periodograms of the RT height, zonal, and meridional wind

632 oscillations for specific months of (a) May 2015 and (b) December 2016. The zonal and

633 meridional wind for (a) is sampled at 9.85 km and (b) at 11 km.

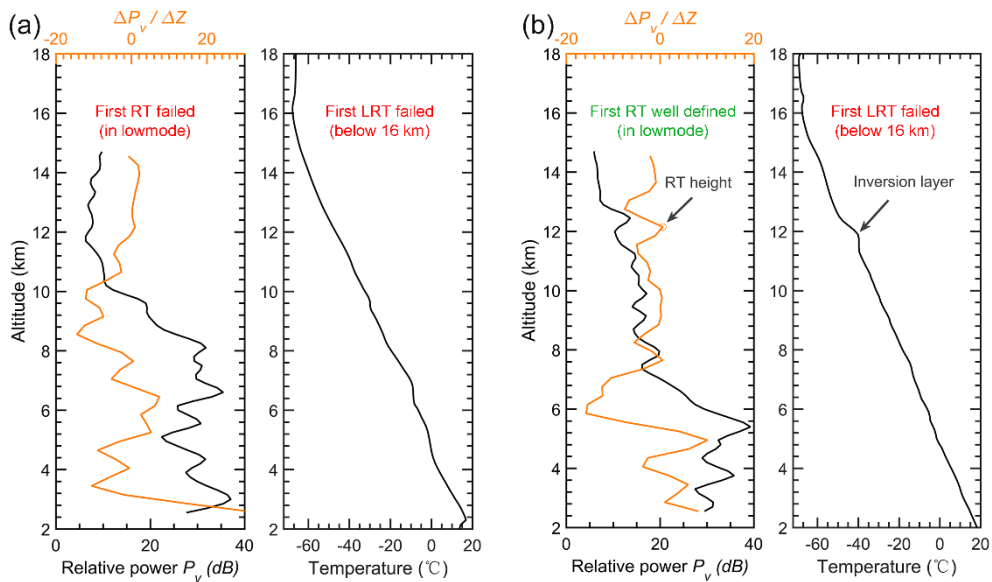
634



635

636 **Figure 11.** Mean Lomb-Scargle periodograms of RT height as a function of the time of

637 month during November 2011-May 2017.



638

639 **Figure 12.** Example profiles of radar echo power and radiosonde temperature that (a)

640 both the RT and LRT definitions fail due to the continuing decrease in temperature on

641 00 UTC 7 July 2012 and (b) the temperature inversion layer failed to meet the LRT

642 definition but well defined in RT definition on 12 UTC 02 August 2012. Please note

643 that we only consider the conditions below 16 km.